University of Nebraska - Lincoln

DigitalCommons@University of Nebraska - Lincoln

1984

Lidar and Balloon-Borne Cascade Impactor Measurements of Aerosols: A Case Study

J. A. Reagan
University of Arizona

M. V. Apte
University of Arizona

T. V. Bruhns
University of Arizona

O. Youngbluth
NASA Langley Research Center, Hampton, VA

Follow this and additional works at: http://digitalcommons.unl.edu/nasapub

Lidar and Balloon-Borne Cascade Impactor Measurements of Aerosols: A Case Study

J. A. Reagan, M. V. Apte, T. V. Bruhns*
Department of Electrical and Computer Engineering, University of Arizona, Tucson, AZ 85721

and O. Youngbluth
NASA Langley Research Center, Hampton, VA 23665

Aerosol size distributions, elemental components, complex refractive indices, extinction profiles and extinction-to-backscatter ratios have been measured and inferred from balloon-borne cascade impactor and lidar observations made during a cooperative joint experiment conducted during the period 4–10 April, 1980 in Tucson, AZ. Size distributions obtained from quartz crystal microbalance (QCM) cascade impactor measurements at different heights (1 to 1000 m) and times over a period of several days were fairly similar in form, being clearly bimodal in their mass distributions with the coarse particle mode being dominant. Electron microscope and energy dispersive X-ray analyses of particles deposited on the QCM stages over the particle radii range ~ 0.5–4.0 μm revealed that the particle samples were elementally dominated by both sulfur and crustal type (Al, Ca, Mg and Si) elements. Complex refractive index estimates for a wavelength of 649 nm were obtained by comparing the lidar inferred aerosol extinction-to-backscatter ratios with theoretically computed values calculated for the impactor-derived size distributions. The real part of the index was estimated to be 1.45 for most cases, while the estimates for the imaginary part ranged between 0.000 and 0.01. Aerosol extinction coefficients calculated for the impactor-derived size distributions were found to be somewhat smaller but in fair agreement with the extinction coefficients retrieved from the lidar measurements.

INTRODUCTION

Considerable effort in recent years has been devoted to the determination of various atmospheric aerosol optical parameters such as extinction, backscatter, scattering phase function and single-scattering albedo. Knowledge of the magnitude and variability of these parameters is critical to an understanding of the influence of aerosols on the radiative transfer of visible and IR radiation within the earth–atmosphere system. Without such knowledge, it is difficult to establish meaningful aerosol environmental standards or to accurately predict how aerosols may effect visibility and climate.

Efforts to determine atmospheric aerosol optical properties have included both the retrieval of optical parameters from optical transmission and scattering measurements and the computations of optical parameters from measurements of physical characteristics such as number density, size distribution, and particle composition. Either of these methods has its own peculiar problems, but if optical parameters are the desired end product, optical measurements seem to offer the most direct approach. Optical sensing techniques can also be applied remotely through the use of natural sunlight or optical sources such as lasers. Moreover, remote sensing techniques offer a viable means for accomplishing the extensive monitoring that would be required to adequately characterize the optical properties of aerosols over extended regions of the earth.

This paper is concerned with the application of laser radar or lidar for the retrieval of

Present affiliation: Hewlett Packard—SID, Palo Alto, CA 94304.

aerosol extinction profiles, and the investigation of related aerosol physical properties which effect the lidar retrieval. Lidar measurements have been made near Tucson over the past three years in a study of the optical properties of atmospheric aerosols in arid regions. Vertical profiles of aerosol extinction and the aerosol extinction to backscatter ratio, S_a, have been determined for about 100 days via the slant-path lidar technique (Spinhirne, Reagan, and Herman, 1980). Successful application of this technique requires aerosol backscatter to be approximately horizontally homogeneous and S_a to be constant with height over the retrieval height interval. Preliminary observations indicate that these requirements are sufficiently well met to permit extinction profile retrievals in Tucson a good fraction of the time (Reagan et al., 1977; Spinhirne, Reagan, and Herman, 1980). To further investigate the effects of various aerosol physical properties on this technique, the present study included intercomparison measurements made with a balloon-borne cascade impactor system, provided through the cooperation of NASA's Langley Research Center. Attempts to conduct the intercomparison experiment were twice thwarted by damage to the balloon system, but a very successful set of balloon and lidar observations were obtained in early April of 1980. The results of these observations are presented in this paper.

INSTRUMENTATION AND SENSING TECHNIQUES

Balloon-Borne Cascade Impactor

The cascade impactor used for the experiment is a quartz crystal microbalance (QCM) cascade impactor (Chuan, 1975), model PC-2, manufactured by California Measurements, Sierra Madre, CA. The QCM consists of ten quartz crystal stages with 50% collection efficiency cutoff radii of 15, 7.5, 3.85, 2.1, 1.0, 0.60, 0.23, 0.13, 0.08 and 0.03 μm for 2 g/cm^3-density spherical particles and a 170 ml/min flow rate. Size separation is accomplished by drawing air in series through the ten stages. Each successive stage contains an inertial impactor jet of decreasing size. Aerosols which impact on the quartz crystal of a given stage remain affixed to the crystal surface by natural adhesion or, in the case of large aerosols, with the aid of a thin, submicron coating of Apiezon grease (by J. G. Biddle Co.) applied to the crystal surface. The crystals are easily removable from the QCM for either cleaning and reusage or retention and subsequent electron microscope analysis of their aerosol deposits.

Each stage of the QCM includes a piezoelectric quartz crystal onto which material is deposited from the impactor jet and a similar reference crystal shielded from the impactor jet. The resonant frequency of the exposed crystal decreases as aerosols accumulate on the crystal. By electronically measuring the change in frequency between the exposed and reference crystals, the mass accumulation of a stage can be monitored as a function of time or total air volume (for a known flow rate). Thus, a mass size distribution may be determined by monitoring the frequency shifts of the different stages for a given time interval. The sensitivity of crystals is sufficiently high ($\sim 10^9$ Hz/g) that quite small changes in mass ($\sim 10^{-9}$ g) can be readily detected. This permits atmospheric distribution measurements to be made in relatively short times even though the flow rate through the impactor is relatively low. For example, a similar QCM has been flown on aircraft to measure aerosols from volcanic eruptions in both the troposphere and stratosphere (Rose et al., 1980; Chuan et al., 1981; Woods and Chuan, 1982).

The tethered balloon system used to carry the QCM aloft and record its output was developed at and provided by NASA's Langley Research Center (Owens et al., 1982). The balloon used with the system is a 100 m^3, helium-filled, class C, model TRF3D-3500, manufactured by Raven Industries, Sioux Falls, S.D. The balloon is moored by a tether cable to a motor-driven winch at the

ground station, which includes the winch and a laboratory hut mounted on a flat-bed trailer and a fair-lead pulley anchored to the ground about 25 m from the trailer. The hut is equipped with a receiving antenna and associated electronics, a computer, and data recording gear to handle signals telemetered from the balloon instrumentation package to the ground station. The instrumentation package is suspended by cable about 15 m below the balloon. It includes the QCM plus the air pump and flow control valve, meteorological sensors for measuring pressure, temperature, humidity, wind speed and wind direction, and transmitting electronics for telemetering the measurements. The balloon and instrumentation package may be moved up or down as rapidly as 0.5 m/sec, and the maximum operational height is about 1500 m AGL (above ground level). Due to Federal Aviation Agency restrictions, balloon soundings for the Tucson experiment were limited to daylight hours and a maximum height of about 1000 m AGL.

Monostatic Lidar

Monostatic or backscatter lidar is analogous to pulsed microwave radar, except that lidar operates in the visible and near visible wavelength region. Pulsed lasers are used as transmitters, and telescope systems serve as receivers. Optical echoes received at any time t after firing the transmitter are related to backscattering at range $r = ct/2$ where c is the speed of light.

The University of Arizona monostatic lidar system used for this experiment is equipped with a 1 J Q-switched ruby laser (wavelength of $\lambda = 694.3$ nm) for the transmitter, and the receiver consists of a 20 cm diameter telescope and RCA 7265 photomultiplier filtered by a 1.2-nm-wide passband. The photomultiplier output is conditioned by a gain-switching amplifier (Spinhirne and Reagan, 1976), and digitized by a Biomation 805 transient recorder. The digitizer output is buffered through an Inter-

data 7/16 minicomputer and stored on 8-inch floppy disks. The laser transmitter output energy is measured each laser shot by a digital energy monitor (Reagan et al., 1976), and the digitized energy value is stored on the floppy disks. The lidar transmitter/receiver assembly is mounted on an altitude-azimuth positioning mount to allow the lidar to be pointed in any specified direction. Digital outputs of the mount-pointing angles are also stored on the floppy disks.

Lidar observations for this experiment consisted of several sets of slant-path measurements. The lidar was fired along a fixed azimuth at several slant or elevation angles ranging from vertically pointing down to an elevation angle 15° above the horizon. A complete slant-path run consisted of measurements at about 10 different slant angles and required 20–30 min to complete. About 10 laser shots were taken at each slant angle to average out the shot noise present in individual lidar returns. Lidar operation was generally restricted to nighttime (just before sunrise or after sunset) because the skylight background typically added too much noise to lidar returns obtained during daylight hours. Thus, some time delay was necessarily incurred between the lidar observations and the balloon measurements.

The atmospheric lidar response or return, $V(r)$, obtained for a given laser shot may be quantitatively described in terms of the lidar equation given by

$$V(r) = \frac{KE_0 \beta(r) T^2(r)}{r^2}, \qquad (1)$$

where $V(r)$ is the instantaneous lidar response due to backscattering at range r, E_0 the transmitted pulse energy, $\beta(r)$ the volume backscattering coefficient at r, $T(r)$ the one-way transmission to r, and K the lidar system calibration constant. The backscatter coefficient in Eq. (1) should actually be interpreted as an average value over some incremental range Δr which has a lower limit of half the laser pulse length but is typically larger as set by the frequency bandpass limi-

tations of the lidar amplifying and digitizing electronics. For the University of Arizona lidar, data are sampled at spatial increments of no less than 30 m because Δr for the system is about 30 m as set by the system electronics.

The transmission, $T(r)$, is related to the unit volume extinction coefficient, $\alpha(r')$, between 0 and r by

$$T(r) = \exp - \int_0^r \alpha(r')\, dr'. \qquad (2)$$

Thus, as can be seen from Eqs. (1) and (2), $\beta(r)$ and $\alpha(r)$ are the basic optical parameters of the atmosphere which determine the nature of the lidar response. These parameters include contributions due to both molecular or Rayleigh scattering and aerosol or Mie scattering (the reader is referred to McCartney (1976) for additional information on atmospheric optical scattering and extinction). The molecular contribution may be computed theoretically from the Rayleigh scattering law, but the aerosol contribution is an unknown, dependent on the aerosol particles present in the atmosphere at the time of the observation. Although Mie scattering strictly applies to spheres, which all aerosol particles are obviously not, it is nonetheless a routinely employed technique to describe aerosol light scattering because it provides a tractable approach for computing scattering by aerosols. Fortunately, the equivalent spherical particle assumption has been found to yield apparently good agreement between theory and observation in many optical scattering experiments (Eiden, 1966; Ward et al., 1973; Grams et al., 1974; Reagan et al., 1977; King et al., 1978; Reagan et al., 1980).

The lidar remote sensing problem is to retrieve the aerosol backscatter and extinction coefficients, $\beta_a(r)$ and $\alpha_a(r)$, from measurements of $V(r)$. This poses an obvious dilemma as there are two unknowns, $\beta_a(r)$ and $\alpha_a(r)$, and only one measurement, $V(r)$, at any range r. This difficulty may be overcome by imposing certain constraints on the problem. As shown by Fernald et al. (1972), if it is assumed that the aerosol extinction-to-backscatter ratio, or S_a ratio, $S_a = \alpha_a/\beta_a$, is constant over some height interval, the lidar equation may be solved to retrieve $\alpha_a(r)$ over that interval. Assuming S_a is constant with height requires that the shape of the aerosol size distribution and the aerosol particle refractive index be height invariant. If the transmission is also known over the height interval, both the value of S_a for the interval and $\alpha_a(r)$ at each point in the interval may be retrieved. The required transmission value may be obtained from lidar returns obtained at different slant angles if the atmosphere is reasonably horizontally homogeneous. Furthermore, by combining lidar returns obtained for several slant angles, it is possible to retrieve S_a, $\alpha_a(r)$ and $T(r)$ simultaneously (Spinhirne et al., 1980). In this approach, slant path lidar measurements are processed by a multiangle integral solution of the lidar equation to extract S_a and vertical profiles $\alpha_a(r)$, $\beta_a(r)$ and $T(r)$. The solution technique assumes S_a is constant with height through layers of aerosol optical thickness (i.e., integrated extinction) of about 0.05 or greater, which corresponds to the entire atmospheric mixing layer for relatively clear conditions. Horizontal homogeneity is required, although horizontal variations in backscatter of 10%–20% at a given height can typically be tolerated without greatly effecting the solution procedure. This is the solution approach which was used to process the lidar observations made during the lidar/balloon experiments.

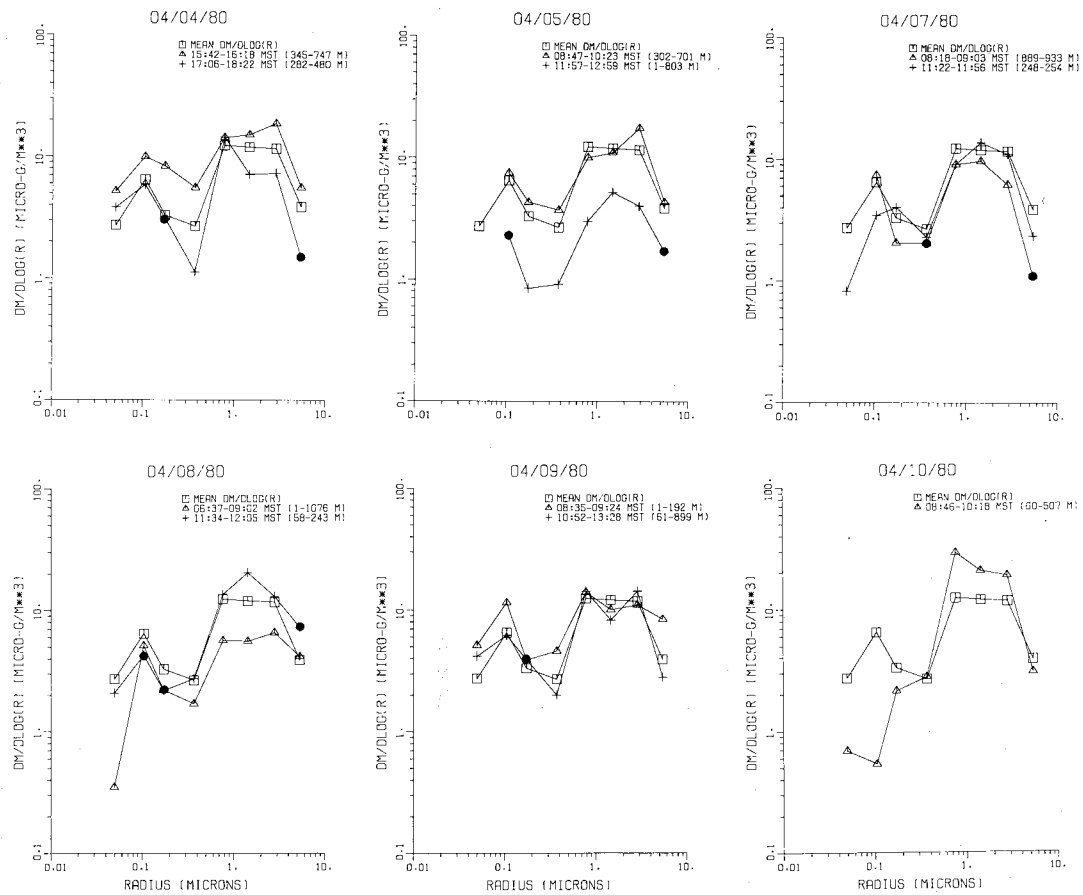## RESULTS AND DISCUSSION

General Conditions

The joint lidar/balloon experiment was conducted over the period 4–10 April, 1980. Observations were made during each day of this period except 6 April. The balloon system was positioned adjacent to the lidar site on the University of Arizona Campbell Avenue Farm at the northern edge of Tucson.
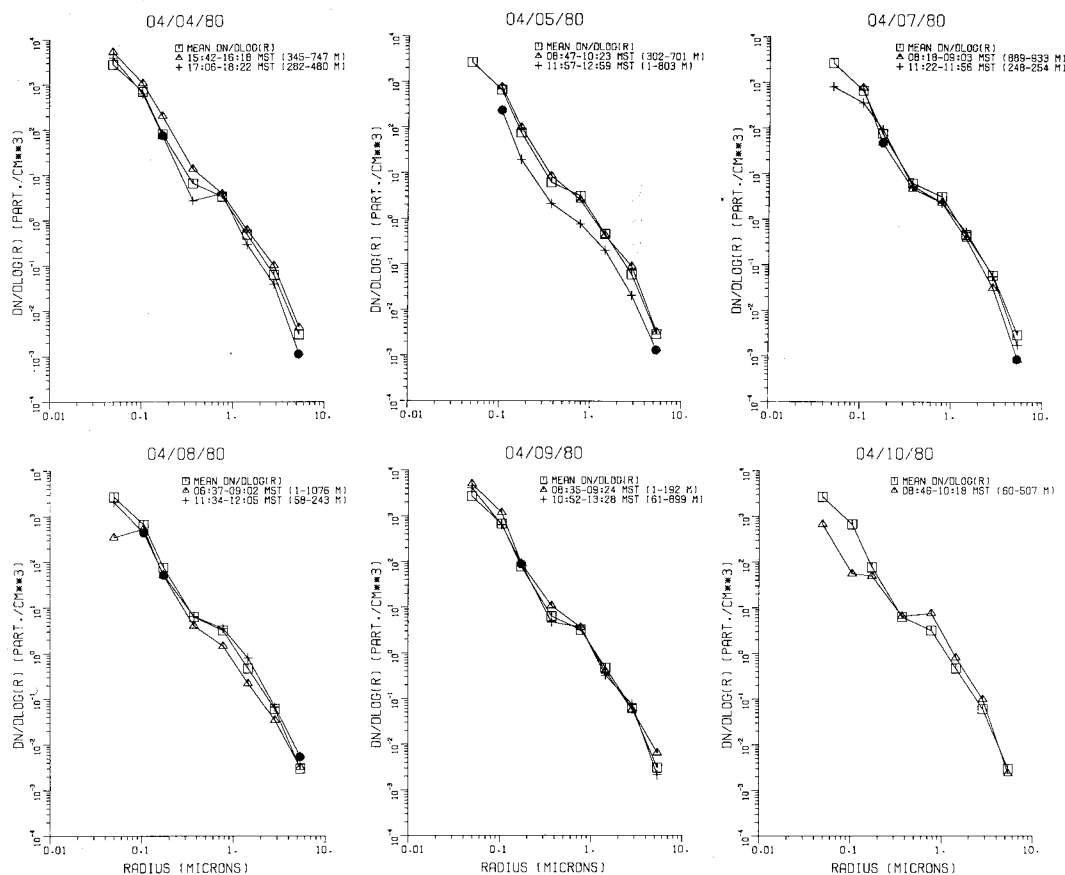
Weather conditions during the experiment were generally mild and clear with only occasional high clouds. A slight warming trend occurred over the period with surface highs ranging between 78° and 86° F and lows between 45° and 52° F. Daily average surface dew points ranged between 21° and 29° F. Surface winds were light to breezy. Tucson was generally under the influence of high pressure systems during this period, but weak, dry cold fronts passed through on 5–6 April and 10 April. Even with the passage of these two rather mild disturbances, diurnal air temperature, dew point temperature and wind patterns remained much the same throughout the period.

FIGURE 1. Mass size distributions derived from impactor measurements.

Cascade Impactor Measurements

Balloon-borne cascade impactor measurements were made at various times and over several different altitude ranges during the course of the experiment. A total of 13 balloon soundings were made over the seven day period, and all but two were successful. One run was lost due to the impactor air-flow valve not being opened before the balloon ascent, and the other due to improper reseating of several of the QCM crystals which had been removed and cleaned after the previous run. The QCM crystals were either cleaned or turned over (either side of a crystal may be used for collection) after each run to provide a clean impaction surface for the next run. A few crystals from selected stages were also removed and stored for subsequent

FIGURE 2. Number density size distributions derived from impactor measurements.

electron microscope analysis of their aerosol deposits.

The mass size distributions obtained from the impactor measurements are given in Figure 1, and the corresponding number density distributions are given in Figure 2. Information about the mass measurements is also given in Table 1. Mean mass and number density distributions, determined from all the distributions, are included in the figures for comparison. The distribution points are plotted at the geometric mean radii of the QCM stages. These radii are determined by the square root of the product of the 50% collection efficiency radii of adjacent stages. The log differentials, $d \log r \approx \Delta \log r$, are de-termined by the difference in the logs of the 50% collection efficiency radii of adjacent stages. The incremental number density, $dN \approx \Delta N$, is determined by assuming the particles contributing to the mass for a particular stage are all at the geometric mean radius of that stage and have a density of 2 g/cm^3. The points shown as solid symbols are for stages which gave spurious readings during a particular balloon run, but were determined from ground-based frequency cross-check measurements made on the QCM before and after a run. These measurements yielded distributions of the same shape as the actual balloon flight measurements in almost every case, and thus appear valid for determining the lost points. However, it must be recognized that these inferred points are not the same as the actual balloon flight measurements.

TABLE 1. Impactor Mass Measurements

Date and time of measurement	Total mass $\mu g/m^3$	Coarse particle mode[a] mass $\mu g/m^3$	Accumulation mode[b] mass $\mu g/m^3$	Relative humidity[c]
4/4/80				
15:42 to 16:18 MST	23.1	14.6 (63%)	8.5	19%–23%
17:06 to 18:22 MST	11.9	7.8 (66%)	4.1	21%–23%
4/5/80				
8:47 to 10:23 MST	15.6	11.6 (74%)	4.0	27%–30%
11:57 to 12:59 MST	4.8	3.9 (81%)	0.9	25%–30%
4/7/80				
8:18 to 9:03 MST	8.2	7.1 (86%)	1.1	37%
11:22 to 11:56 MST	13.0	10.0 (77%)	3.0	33%
4/8/80				
6:37 to 9:02 MST	8.4	6.0 (71%)	2.4	30%–60%
11:34 to 12:05 MST	18.5	15.0 (81%)	3.5	25%–28%
4/9/80				
8:35 to 9:24 MST	18.8	11.5 (61%)	7.3	26%–37%
10:52 to 13:28 MST	14.9	10.3 (69%)	4.6	19%–23%
4/10/80				
8:46 to 10:18 MST	21.0	18.9 (90%)	2.1	24%–34%

[a]Coarse particle mode mass determined by sum of masses on QCM stages for radii $> 0.5\mu m$.
[b]Accumulation mode mass determined by sum of masses on QCM stages for radii $< 0.5\mu m$.
[c]The relative humidity range for the height interval of the impactor measurements as determined from measurements made with dry and wet bulb temperature sensors on the balloon system.

Regarding the accuracy that can be attached to any of the distribution points, the QCM sensitivity is such that the smallest mass measurement included here should not be uncertain by more than about ±15%. Added errors due to the aerosols not being of density 2 g/cm³ or perfect spheres cannot be readily specified, but such effects can significantly alter the values of the radii assumed for the distribution points. We would be less than candid if we did not acknowledge that such effects could cause uncertainties in the effective number density determinations easily amounting to a factor of two.

The shapes and significant features of the size distributions in Figures 1 and 2 are generally rather similar even though the measurements were made at different times and various altitude ranges over several days. The continuity, slope trends, etc. in the distributions indicate few if any disparate points that might be regarded as significantly off or out of place. The mass distributions clearly reveal both the large or coarse particle mode and the smaller accumulation mode. The coarse particle mode is consistently larger, although the relative amounts of mass in the two modes does vary somewhat between different runs. This variation does not appear to be correlated with the total particle mass. The dominance of the coarse particle mode is revealed by the consistent lump in the number density distributions starting at about 0.4 μm in particle radius. The general shape of the number density distributions is quite similar to many of those we have obtained previously from both direct aircraft measurements (Reagan et al., 1977) and mathematical inversions of solar radiometer

spectral extinction and laser angular scattering data (King et al., 1978; Reagan et al., 1980).

Electron Microscope Analysis

Crystals from stages 6, 5 and 4 (geometric mean radii of 0.75, 1.42 and 2.69 μm, respectively) of the QCM were replaced after each day's balloon runs, and removed crystals were stored for later analysis by electron microscope. These stages all are in the coarse particle mode. They were selected primarily because they fall in the particle size range which typically contributes the greatest amount to the aerosol backscatter coefficient, β_a. In retrospect, it would have been informative to have also selected at least one crystal from the accumulation mode size range.

Scanning electron microscope (SEM) analyses of the crystals retained from the experiment were performed both at NASA's Langley Research Center and at the Stanford Research Institute (courtesy of R. L. Chuan, Brunswick Corp.). In addition to obtaining SEM photomicrographs of the impacted particles, the crystals were also subjected to energy dispersed X-ray (EDX) analysis to identify the elemental composition (for elements with atomic number 11 and up) of the particles.

Example SEM photographs of particles collected on some of the days during the experiment are given in Figure 3. The darkened areas are caused by particle shadowing rather than any staining from the particles. The photographs reveal that the particles are generally fairly uniform in size and within the size collection range appropriate to the QCM stage in question. Some particles appear too large or small for the stage they were collected on, presumably because of significant density or aerodynamics shape differences for these particles. Although the particles are generally nonspherical, the majority could be encircled by ellipses with major to minor axis ratios of

two or less. Thus, most of the particles do not appear to be grossly nonspherical.

Results of the EDX analysis performed at the Stanford Research Institute are given in Table 2. Scans were made of individual particles collected on QCM stages 5 and 6 during the balloon run made on 10 April, 1980. The areas which were scanned on stage 6 are identified in the photograph given in Figure 4. Scan profiles for some of these areas are also included in the figure. The high incidence of Al detection, and to a lesser extent Ca, Fe and Mg, suggests that the sampled particles are largely crustal in origin (Moyers et al., 1977). It is perhaps surprising that S was detected as frequently as Al. Sulfate particles are to be expected in the submicron accumulation mode (Whitby, 1978); they have been found to be a significant constituent of the fine particle population even in remote background areas of the world (Bigg, 1980; Cunningham and Zoller, 1981; Winchester et al., 1981). Previous aircraft aerosol measurements (Reagan et al., 1977) made around Tucson also revealed that the submicron particle samples were dominated by acid-sulfate particles. The S detected in the coarse mode particles collected during this experiment can possibly be attributed to sulfur compounds forming on or attaching to the larger, crustal particles. A high incidence of Si is also to be expected in view of the desert location of the measurements and the high incidence of other crustal elements (Moyers et al., 1977; Pitchford et al., 1981). As shown in Table 2, Si was typically only present in trace amounts. However, this may be misleading because Si, Ag, Cr and Ni are all background elements contained in the QCM crystals or crystal contacts. Their background contribution must be subtracted to determine whether they are also present in a particle. When the background contribution is particularly strong, as in the case of Si, it can be difficult to discern whether an element is really present. Thus, the trace indications for Si may actually correspond to more significant amounts of Si in the

a)

b)

⊢—⊣
5 μm

c)

d)
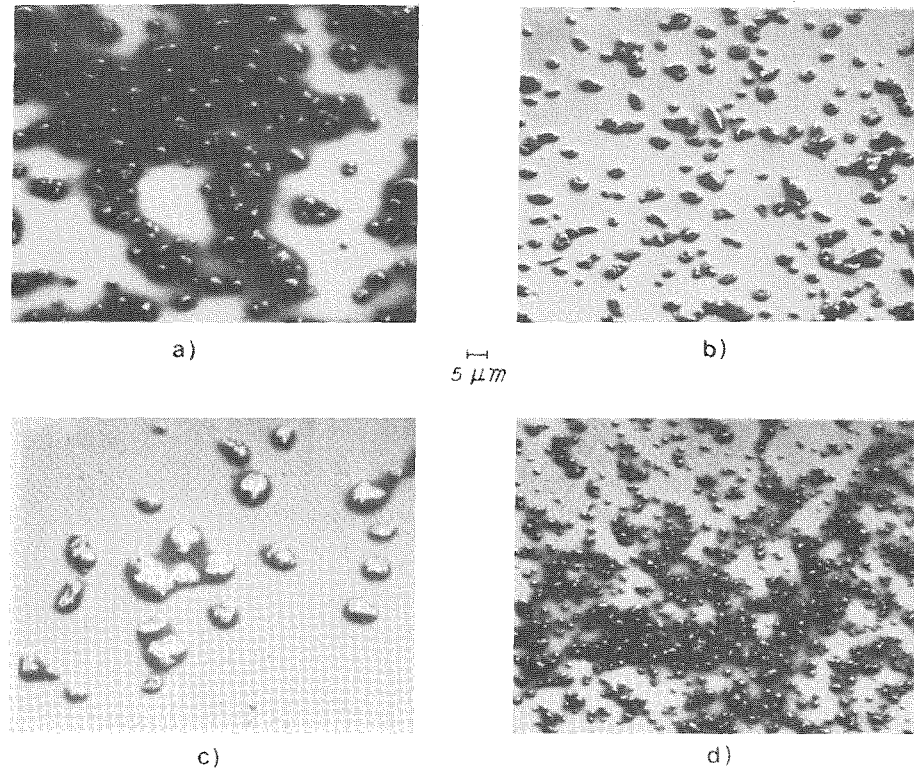
FIGURE 3. Photomicrographs of particles collected on QCM stages: (a) QCM stage 5 for 5 April 8:47–12:39 MST, (b) QCM stage 5 for 7 April 11:22–11:56, (c) QCM stage 4 for 9 April 10:52–13:28 MST, and (d) QCM stage 6 for 9 April 16:24–19:00 MST.

particles. The EDX scans made at NASA's Langley Research Center did not include background subtraction, so they cannot provide an indication of Si. However, these scans did reveal the presence of Al, Ca, Mg and S for all other days that impactor measurements were made. Thus, the results given in Table 2 appear to be fairly representative of the particles present on other days of the experiment.

Lidar Measurements

Aerosol extinction profiles obtained from the slant-path lidar measurements made during the experiment are given in Figures 5, 6 and

7. The heights are all AGL (above ground level), and the Rayleigh or molecular extinction profile is included for comparison. Error bars ($\pm$ one standard deviation) are included to indicate the estimated uncertainty of the extinction profile within the mixing layer. Table 3 lists the aerosol extinction to backscatter ratio, S_a, mixing layer height, mixing layer optical depth and total optical depth (actually optical depth to a height of 19.3 km) associated with each of the extinction profiles. The majority of the extinction profile retrievals yielded fairly low extinction standard deviations ($\sim \pm 15\%$) for the mixing layer, which is an indication that the requirements that horizontal homogeneity in β_a and S_a be constant with height were reasonably well met (Spinhirne et al., 1980). The poorest accuracy ($\sim \pm 50\%$) was obtained for 5 April, which is to be expected because of the very clean conditions indicated by the low mixing layer optical depth and total

TABLE 2. Summary of Elemental Analysis by EDX of Individual Particles on QCM Stages 5 and 6 for Impactor Measurements on 10 April, 1980, 8:46 to 10:18 MST

| Elements detected	Points scanned in stage 5[a]						Points scanned in stage 6[a]				
	A	B	C	D	E	F	A	B	C	D	E
Ag[b]	P	—	P	—	P	—	P	—	P	—	T
Al	P	P	P	—	P	P	P	P	—	P	P
Ca	P	—	P	—	P	P	T	P	P	P	—
Cl	—	—	—	—	—	—	P	—	—	—	P
Cr[b]	T	T	T	T	T	T	T	T	T	T	T
Fe	—	T	T	—	T	T	—	P	—	—	—
K	—	—	—	P	—	P	—	P	—	—	—
Mg	P	T	T	—	T	T	—	P	P	—	—
Na	—	—	—	—	—	—	—	—	—	—	P
Ni[b]	—	—	T	T	T	T	—	T	T	T	—
P	—	—	—	—	—	—	—	—	P	—	—
S	P	P	—	P	P	P	P	P	P	—	P
Si[b]	T	T	T	T	T	T	—	P	—	P	T

P = element clearly detected, T = trace of element detected, and — = element not detected.
[a]Stage 6 has a geometric mean radius of 0.75 μm and Stage 5 of 1.42 μm.
[b]Elements Ag, Cr, Ni and Si are in QCM crystal and crystal contacts and thus show up strongly in background.

FIGURE 4. Photomicrograph of particles collected on QCM stage 6 for 10 April 8:46–10:18 MST. Areas labeled A, B, C, D and E subjected to EDX analysis; EDX scans are included for areas B and C.
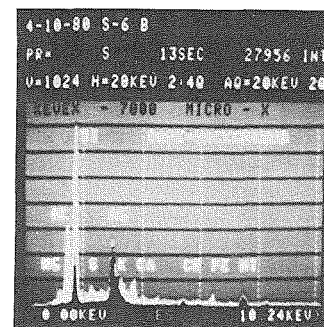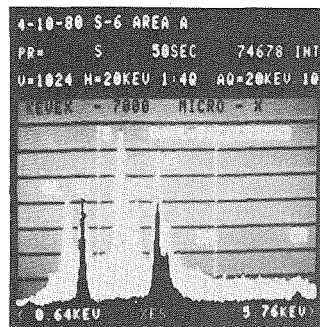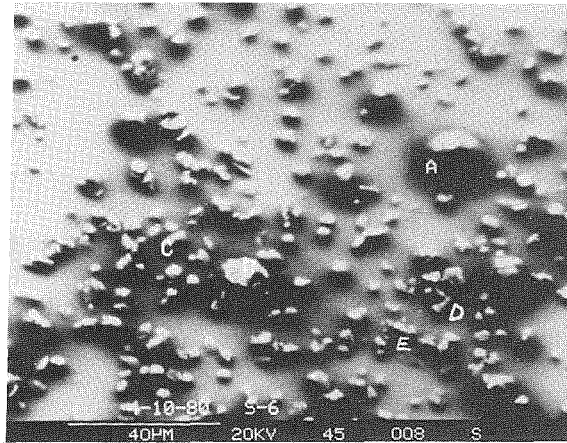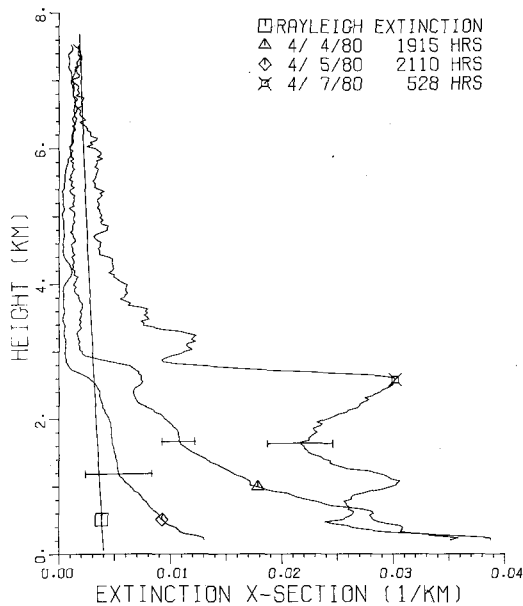
FIGURE 5. Aerosol extinction profiles for lidar measurements on 4, 5, and 7 April. Time of measurements in MST included in figure.
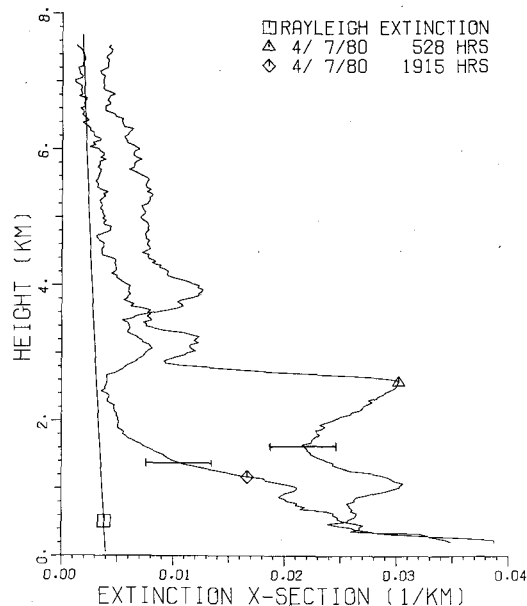
FIGURE 6. Aerosol extinction profiles for lidar measurements on 7 April. Time of measurements in MST included in figure.

FIGURE 7. Aerosol extinction profiles for lidar measurements on 8, 9 and 10 April. Time of measurements in MST included in figure.
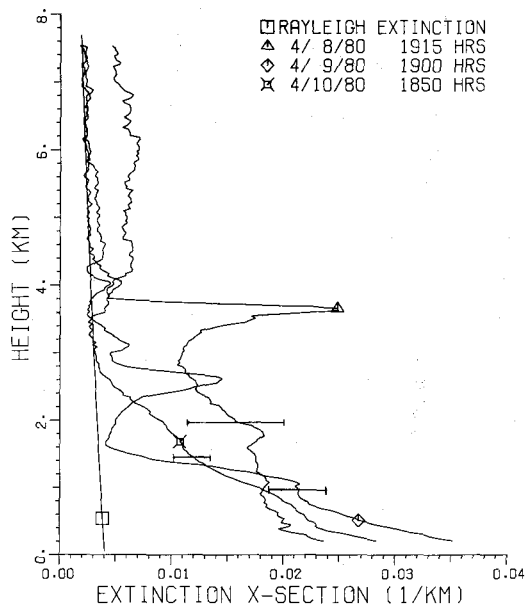
optical depth for that day. The retrieval technique simply yields less accurate results when the aerosol contribution to the lidar signal becomes a smaller fraction of the total, aerosol plus Rayleigh, signal. The fact that the aerosol extinction for 5 April is quite small compared to the Rayleigh level for heights above the mixing layer provides an indication that the lidar calibration constant has been determined fairly accurately (Spinhirne et al., 1980). The errors for the 7 April pm and 8 April extinction profiles are somewhat larger ($\sim \pm 25\%$) than the majority of the profiles, even though the optical depths are rather high for these days. This is most likely due to poorer horizontal homogeneity in β_a at the time the lidar observations for these profiles were made.

The lidar derived optical depths are plotted in Figure 8, along with aerosol optical depths obtained for some of the days from measurements made with the University of Arizona's spectral solar radiometer

TABLE 3. Results of Lidar Measurements

Day	Mixing layer height (km)	Aerosol optical depth to top of mixing layer	Total aerosol optical depth[a]	Aerosol extinction to backscatter ratio S_a
4/4/80	3.0	0.050 ± 0.007	0.066 ± 0.008	23.1 ± 4.1
4/5/80	2.8	0.018 ± 0.009	0.028 ± 0.010	10.8 ± 6.1
4/7/80 AM	2.9	0.079 ± 0.014	0.100 ± 0.017	40.0 ± 6.0
4/7/80 PM	4.4	0.060 ± 0.015	0.094 ± 0.018	38.8 ± 6.5
4/8/80	3.8	0.062 ± 0.022	0.099 ± 0.027	37.4 ± 8.3
4/9/80	2.8	0.046 ± 0.007	0.070 ± 0.009	26.8 ± 6.0
4/10/80	2.9	0.042 ± 0.006	0.061 ± 0.007	22.6 ± 4.1

[a]Total optical depth is only to a height of 19.3 km, but this typically includes most of the optical depth contribution.

(Shaw, et al., 1973; King et al., 1980). The solar radiometer optical depth measurements provide a cross check to verify the lidar extinction retrieval. The radiometer optical depth value for 6 April falls in about the right place for the increasing trend indicated by the lidar values over the period 5–8 April, the 8 April value is definitely a little lower

FIGURE 8. Lidar and solar radiometer aerosol optical depth measurements for various days during experiment. Error bars are ± one standard deviation.
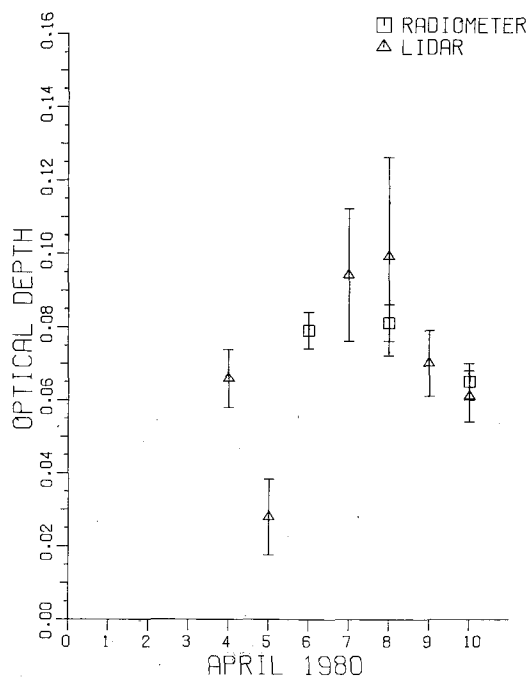
than, but within the error limits of, the lidar value, and the 10 April value is very close to the lidar value. Thus, while it was not possible to obtain solar radiometer data for more days during the experiment, the data that were obtained agree fairly well with the lidar data.

A number of interesting features are apparent from the lidar data. For example, the extinction profiles demonstrate the significant day to day variations in extinction, both in magnitude and vertical structure, that occurred during the experiment. Some consistency in extinction values is apparent in the lowest few hundred meters. Mixing layer heights did not vary greatly from day to day, which is as expected for the fairly constant temperature and sunshine conditions that prevailed throughout the measurement period. A significant reduction in aerosols occurred on 5 April, 1980 as indicated by the reduced extinction (Figure 5), reduced optical depth (Figure 8), and reduced size distributions (at noon compared to morning, Figures 1 and 2) for that day. This event occurred at about the same time that a weak, dry cold front passed over Tucson, but a similar front with similar trajectories passed through on 10 April, 1980 without any corresponding great change in these same aerosol properties.

The behavior of the aerosol extinction to backscatter ratio, S_a, is of particular interest. The pattern displayed by S_a during the experiment is similar to what we have observed

in general, namely, that the majority of the time S_a falls in the range 20–30, a less frequent grouping occurs in the range 35–60, and on rare occasions S_a drops to less than 15. That S_a varied as it did during the experiment is fortuitous, because one of the objectives of the experiment was to identify causes of changes in S_a.

As noted earlier, S_a depends on the shape or form of the aerosol size distribution and on the aerosol particle refractive index (i.e., on particle composition). Particle shape also has some influence, apparently causing S_a to increase as particles become more nonspherical (Reagan and Herman, 1980). However, within the limitations of spherical particle or Mie scattering theory, only the effects of size distribution form and particle refractive index can be readily assessed. Additional complications still arise even with the spherical particle restriction because particle compositions may be inhomogeneous both within a single particle and as a function of particle size. Assuming the particles to be modeled by a single, average refractive index value is an obvious compromise. Scattering computa-

tions for polydispersions of spherical, inhomogeneous particles can produce significantly different values for various optical parameters depending on how the different constituents which the particles are comprised of are mixed or averaged (Gillespie et al., 1978; Ackerman and Toon, 1981; Sloane, 1983). Nonetheless, our approach in assessing the observed S_a values is to apply the spherical, homogeneous particle assumptions and see if the observations can be reasonably explained by this level of analysis, instead of first attempting something more complicated.

Theoretical Mie scattering computations of α_a and β_a, to determine $S_a = \alpha_a/\beta_a$, were made for each of the impactor-derived size distributions given in Figure 2. The calculations were made for a wavelength of 649.3 nm and particle refractive index, m, values including real components of 1.40, 1.45, 1.50 and 1.54, and imaginary components of 0.000, 0.005, and 0.010. The resulting array of computed S_a values for each distribution was then compared to the S_a value derived from lidar measurements made closest in

TABLE 4. Calculated[a] Values of S_a for Different Impactor Size Distribution Measurements

For impactor measurements on 4/5/80 11:57 to 12:59 MST			
	m Imaginary		
m Real	0.000	0.005	0.010
1.40	29.2	47.6	63.8
1.45	24.6	37.0	47.8	Lidar $S_a = 10.8 \pm 6.1$
1.50	16.2*	23.2	29.6
1.54	**11.5***	16.1*	20.7

For impactor measurements on 4/7/80 8:18 to 9:03 MST			
	m Imaginary		
m Real	0.000	0.005	0.010
1.40	33.5	49.7	63.8
1.45	25.0	35.3*	**44.4***	Lidar $S_a = 40.0 \pm 6.0$
1.50	15.8	21.3	26.7
1.54	10.6	14.7	18.6

[a]Calculations made by numerical evaluation of the Mie volume backscattering and extinction coefficients for a wavelength of 694.3 nm, a particle radius range extending from 0.05 to 6.0 μm, and the refractive index values indicated in the table.

time to each impactor size distribution measurement. Example calculations for some of these cases are given in Table 4. Tabular values with asterisks identify calculated S_a values falling within ± one standard deviation of the lidar S_a value, and the boldfaced entry denotes the optimum or best fit value (i.e., calculated value closest to the lidar value). Correspondingly, the refractive index for this optimum value is taken as the optimum refractive index estimate.

Table 5 lists the optimum refractive index estimates for each lidar S_a value obtained during the experiment. The same refractive index estimates are obtained if the mean size distribution of all the impactor runs (mean is shown in Figures 1 and 2) is used rather than the particular distribution for each impactor run made closest to the lidar measurement. Thus, the observed day to day changes in S_a appear primarily due to refractive index or compositional changes in the particles. The high S_a values on 7–8 April appear to be due to the combined effects of both a reduced real component and a nonzero imaginary component. The low real refractive index value (1.45) is indicative of liquid particles, and, considering the low relative humidities (RH < 40%) which persisted during the experiment, acid sulfate particles or particle coatings present a possible explanation for the inferred index value. Similar low values of the real component have been inferred from previous lidar-solar radiometer measurements (Reagan et al., 1980), and particle

samples collected by aircraft during some of these measurements were found to include a substantial fraction of sulfuric acid type particles (Reagan et al., 1977). On the other hand, a real component value in the 1.45–1.50 range is also representative of some soil and dust models (Gillespie, Jennings, and Lindberg, 1978; Ackerman and Toon, 1981; Clark and Waggoner, 1982) assumed for aerosols. Only one day, 5 April, when the extinction was very low, yielded a high real component (1.54) consistent with ammonium sulfate and silica which are so frequently named as chief aerosol constituents. The imaginary component estimates determined from the data (average of 0.004) are in agreement with values obtained for the 500–700 nm wavelength range from a number of other desert aerosol experiments (e.g., De Luisi et al., 1970; Grams et al., 1974; Lindberg and Laude, 1974; Reagan et al., 1980; Spinhirne et al., 1980). Although imaginary indices in the range of 0.001–0.01 do not correspond to any specific substance commonly associated with atmospheric aerosols, the occurrence of values in this range is possibly a result of small amounts of carbon mixing with otherwise very weakly absorbing particles (Lindberg and Gillespie, 1977; Ackerman and Toon, 1981).

The theoretical calculations of aerosol extinction, α_a, used in the determination of S_a may also be compared with the lidar-derived extinction profiles. Such a comparison should only be regarded as an approximate con-

TABLE 5. Estimated Values of Refractive Index Obtained from Impactor and Lidar Measurements

Date and time of impactor measurement		Lidar S_a	Estimated refractive index m
4/4/80	17:06–18:22 MST	23.1 ± 4.1	1.45 − 0.000i
4/5/80	11:57–12:59 MST	10.8 ± 6.1	1.54 − 0.000i
4/7/80	8:18–9:03 MST	40.0 ± 6.0	1.45 − 0.010i
4/7/80	11:22–11:56 MST	38.8 ± 6.5	1.45 − 0.005i
4/8/80	11:34–12:05 MST	37.4 ± 8.3	1.45 − 0.005i
4/9/80	10:52–13:28 MST	26.8 ± 6.0	1.50 − 0.010i
4/10/80	8:46–10:18 MST	22.6 ± 4.1	1.45 − 0.000i

Average real component = 1.47; average imaginary component = 0.004

sistency check because the balloon and lidar measurements were not made simultaneously. Advection and vertical mixing could cause substantial changes in extinction at any given height in a matter of a few hours. Table 6 lists the α_a values used in the determination of S_a as discussed earlier. The refractive index values assumed for these α_a values are those listed in Table 5, but the particular choice of index is not too critical because α_a does not vary much for the range of index values considered here. Height-averaged lidar α_a values are also included in the table. The lidar and calculated α_a values are in agreement by a factor of 2.75 or less in all cases and on the average within a factor of 2.2. This level of agreement, in an absolute sense, is not too bad, considering the time difference in the observations as well as the uncertainties in the lidar and impactor measurements. Several of the balloon runs also include heights below 200 m above ground, which is closer to the ground than the lidar retrievals can extend because of initial nonoverlap of the lidar transmitter and receiver beams. Nevertheless, it is disconcerting that the lidar values are consistently larger by

about a factor of 2.2. This naturally prompts the thought of a possible scale factor error in determining the number density distribution values from the impactor mass measurements or in computing α_a from these distributions and the Mie scattering coefficients. However, careful rechecking revealed no such scaling errors. Another possible source of error is the lidar calibration. This can be cross checked both by checking how well the lidar and solar radiometer total optical depths agree and by checking how small the aerosol extinction becomes relative to the Rayleigh extinction at heights well above the mixing layer. Either of these checks do not indicate any significant problems. Only the lidar profile for 8 April appears to have a large extinction value above the mixing layer and a somewhat larger total optical depth than the solar radiometer value. As the same calibration constant was applied to all the lidar data, there is no reason to believe that this day should be any more in error due to calibration uncertainties than any of the other days. Moreover, the disagreement in α_a values is about the same for 8 April as for the other days. Thus, while it would be more

TABLE 6. Calculated Values of α_a for Different Impactor Size Distribution Measurements and Corresponding Lidar Determinations of α_a

Date, time and height interval of impactor measurement		Computed α_a (km^{-1})	Average[a] lidar α_a (km^{-1})
4/4/80	17:06–18:22 MST 282–480 m	0.011	0.030 ± 0.006
4/5/80	11:57–12:59 MST 1–800m	0.004	0.0010 ± 0.005
4/7/80	8:18–9:03 MST 889–933m	0.010	0.027 ± 0.005
4/7/80	11:22–11:56 MST 248–254 m	0.012	0.032 ± 0.009
4/8/80	11:34–12:05 MST 58–243 m	0.014	0.025 ± 0.008
4/9/80	10:52–13:28 MST 61–899 m	0.013	0.026 ± 0.004
4/10/80	8:46–10:18 MST	0.020	0.025 ± 0.004

[a]Lidar extinction value for profile from Figures 5, 6, or 7 nearest in time to the impactor measurement and averaged over height interval, to the extent possible, of the impactor measurement.

satisfying if the lidar and impactor derived values of α_a were in closer agreement, the discrepancy is not sufficiently large to indicate that any problem really exists.

SUMMARY

Results have been presented from an experimental study of atmospheric aerosols performed near Tucson which incorporated both lidar and balloon-borne cascade impactor measurements. Aerosol size distributions obtained from the impactor data were found to be all rather similar in form even though the impactor measurements were made at different heights and times over a period of several days. The distributions displayed a dominance by coarse mode particles and were similar to distributions obtained previously in Tucson from other direct sampling and optical remote sensing measurements.

Aerosol extinction profiles and extinction-to-backscatter ratios obtained from the lidar measurements displayed significant changes over the several days of the experiment. The standard deviations obtained for the extinction profiles were generally low (15%–30%) and indicated that the homogeneity constraints on the lidar extinction retrieval technique were reasonably well met. By combining the lidar-derived aerosol extinction-to-backscatter ratios and the impactor size distribution determinations, an estimate was obtained of the aerosol particle refractive index for each lidar observation. This analysis indicated that the observed day to day variations in the aerosol extinction-to-backscatter ratio were largely due to changes in the particle refractive index, rather than to a change in the shape of the aerosol size distribution.

The real part of the estimated refractive index (for a wavelength of 649 nm) was typically 1.45 with a mean of 1.47. This value is reconcilable with both acid sulfate and soil type particles. Energy dispersive X-ray analysis of the particles deposited on the impactor stages for particle sizes contributing most

significantly to the lidar signal revealed that the particles contained both sulfur and soil type elements. Estimates of the imaginary index component (again for a wavelength of 694 nm) ranged between 0.000 and 0.010. Imaginary index values of 0.01 or less are in agreement with values obtained for the 500 to 700 nm wavelength range from a number of other desert aerosol experiments. As sulfur and soil type particle constituents are largely nonabsorbing in this wavelength range, the nonzero imaginary index values may be due to minute amounts of soot intermixed with the other particle components. Finally, the lidar measurements yielded aerosol extinction values that were somewhat higher but still in fair agreement with the aerosol extinction coefficients computed from the impactor size distribution measurements.

REFERENCES

Ackerman, T. P., and Toon, O. B. (1981). Absorption of visible radiation in atmosphere containing mixtures of absorbing and nonabsorbing particles, *Appl. Opt.* 20:3661–3667.

Bigg, K. E. (1980). Comparison of aerosol at four baseline atmospheric monitoring stations, *J. Appl. Meteor.* 19:521–533.

Chuan, R. L. (1975). Rapid measurements of particulate size distribution in the atmosphere, in *Fine Particles-Aerosol Generation, Measurement, Sampling and Analysis* (B. Y. H. Liu, Ed.), Academic Press, New York, p. 763.

Chuan, R. L., Woods, D. C., and McCormick, M. P. (1981). Characterization of aerosols from eruptions of Mount St. Helens, *Science* 211:830–832.

Clarke, A. D., and Waggoner, A. P. (1982). Measurements of particle optical absorption, imaginary refractive index, mass concentration, and size at First International LAAP Workshop, *Appl. Opt.* 21:398–402.

Cunningham, W. C., and Zoller, W. H. (1981). The chemical composition of remote area aerosols, *J. Aerosol Sci.* 12:367–384.

De Luisi, J. J., Furakawa, P. M., Gillette, D. A., Schuster, B. G., Charlson, R. J., Porch, W. M., Fegley, R. W., Herman, B. M., Rabinoff, R. A., Twitty, J. T., and Weinman, J. A. (1976). Results of a comprehensive atmospheric aerosol-radiation experiment in the southwestern United States. Part II: Radiation flux measurements and theoretical interpretation. *J. Appl. Meteor.* 15:455–463.

Eiden, R. (1966). The elliptical polarization of light scattered by a volume of atmospheric air, *Appl. Opt.* 5:569–575.

Fernald, F. G., Herman, B. M., and Reagan, J. A. (1972). Determination of aerosol height distributions by lidar, *J. Appl. Meteor.* 11:482–499.

Gillespie, J. B., Jennings, S. G., and Lindberg, J. D. (1978). Use of an average complex refractive index in atmospheric propagation calculations, *Appl. Opt.* 17:989–991.

Grams, G. W., Blifford, I. H. Jr., Gillette, D. A., and Russell, P. B. (1974). Complex index of refraction of airborne soil particles, *J. Appl. Meteor.* 13:459–471.

King, M. D., Byrne, D. M., Herman, B. M., and Reagan, J. A. (1978). Aerosol size distributions obtained by inversion of spectral optical depth measurements, *J. Atmos. Sci.* 35:2153–2167.

King, M. D., Byrne, D. M., Reagan, J. A., and Herman, B. M. (1980). Spectral variation of optical depth at Tucson, Arizona between August 1975 and December 1977, *J. Appl. Meteor.* 19:723–732.

Lindberg, J. D., and Gillespie, J. B. (1977). Relationship between particle size and imaginary refractive index in atmospheric dust, *Appl. Opt.* 16:2628–2630.

Lindberg, J. D., and Laude, L. S. (1974). Measurement of the absorption coefficient of atmospheric dust, *Appl. Opt.* 13:1923–1927.

McCartney, E. J. (1976). *Optics of the Atmosphere.* Wiley, New York, p. 1.

Moyers, J. L., Ranweiler, L. E., Hopf, S. B., and Korte, N. E. (1977). Evaluation of particulate trace species in southwest desert atmosphere, *Environ. Sci. Technol.* 11:789–795.

Owens, T. L., Storey, R. W., and Youngbluth, O. (1982). NASA Langley Research Center Tethered Balloon System, NASA TM-83260.

Pitchford, M., Flocchini, R. G., Draftz, R. G., Cahill, T. A., Ashbaugh, L. L., and Eldred, R. A. (1981).

Silicon in submicron particles in the southwest, *Atmos. Environ.* 15:321–333.

Reagan, J. A., Byrne, D. M., King, M. D., Spinhirne, J. D., and Herman, B. M. (1980). Determination of the complex refractive index and size distribution of atmospheric particulates from bistatic-monostatic lidar and solar radiometer measurements, *J. Geophys. Res.* 85:1591–1599.

Reagan, J. A., and Herman, B. M. (1980). Light scattering by irregularly shaped particles versus spheres: What are some of the problems presented in remote sensing of atmospheric aerosols?, in *Light Scattering by Irregularly Shaped Particles* (D. W. Schuerman, Ed.). Plenum Press, New York, p. 319.

Reagan, J. A., Spinhirne, J. D., Bruhns, T. V., and Peck, R. L. (1976). Digital detector for monitoring lidar output energy, *Rev. Sci. Instrum.* 47:1527–1530.

Reagan, J. A., Spinhirne, J. D., Byrne, D. M., Thomson, D. W., de Pena, R. G., and Mamane, Y. (1977). Atmospheric particulate properties inferred from lidar and solar radiometer observations compared with simultaneous in situ aircraft measurements: A case study, *J. Appl. Meteor.* 16:911–928.

Rose, W. I. Jr., Chuan, R. L., Cadle, R. D., and Woods, D. C. (1980). Small particles in volcanic eruption clouds, *Amer. J. Sci.* 280:671–696.

Shaw, G. E., Reagan, J. A., and Herman, B. M. (1973). Investigations of atmospheric extinction using direct solar radiation measurements made with a multiple wavelength radiometer, *J. Appl. Meteor.* 12:374–380.

Sloane, C. S. (1983). Optical properties of aerosols-comparisons of measurements with model calculations, *Atmos. Environ.* 17:409–416.

Spinhirne, J. D., and Reagan, J. A. (1976). Gain-switching amplifier for compression of optical radar return signals, *Rev. Sci. Instrum.* 47:437–439.

Spinhirne, J. D., Reagan, J. A., and Herman, B. M. (1980). Vertical distribution of aerosol extinction cross section and inference of aerosol imaginary index in the troposphere by lidar technique, *J. Appl. Meteor.* 19:426–438.

Ward, G., Cushing, K. M., McPeters, R. D., and Green, A. E. S. (1973). Atmospheric aerosol index of refraction and size-altitude distribution from bistatic laser scattering and solar aureole measurements, *Appl. Opt.* 12:2585–2592.

Whitby, K. T. (1978). Physical characteristics of sulfur aerosols, *Atmos. Environ.* 12:135–159.

Winchester, J. W., Weixiu, L., Lixin, R., Mingxing, W., and Maenhaut, W. (1981). Fine and coarse aerosol composition from a rural area in north China, *Atmos. Environ.* 15:933–937.

Woods, D. C., and Chuan, R. C. (1982). Fine particles in the Soufriere eruption plume, *Science* 216:1118–1119.